Catalytic Phosphoryl Interactions of Topoisomerase IB†

Rajesh Nagarajan,‡ Keehwan Kwon,‡,§ Barbara Nawrot,|| Wojciech J. Stec,|| and James T. Stivers*,‡

Department of Pharmacology and Molecular Sciences, The Johns Hopkins University School of Medicine, 725 North Wolfe Street, Baltimore, Maryland 21205-2185, and Department of Bioorganic Chemistry, Centre of Molecular and Macromolecular Studies, Polish Academy of Sciences, Lodz, Poland

Received April 29, 2005; Revised Manuscript Received June 25, 2005

ABSTRACT: The reversible nucleophilic substitution reaction catalyzed by the vaccinia virus type IB topoisomerase has been investigated by measuring the equilibrium and rate effects of stereospecific sulfur substitution at the two nonbridging oxygen atoms of the attacked phosphodiester group. An energetic analysis of the combined effects of sulfur substitution and site-directed mutagenesis of active site residues of the enzyme has identified enzyme interactions with each oxygen in the ground state and transition state. We use these findings in combination with previous structural and 5′-bridging sulfur substitution results to deduce the web of enzymatic interactions with the nonbridging oxygens as well as the 5′-hydroxyl leaving group. A key finding is the central role of Arg130, which forms electrostatic interactions with both nonbridging oxygens and the 5′-leaving group.

The type IB DNA topoisomerases (Topo)[1] of eukaryotic viruses and mammals catalyze a reversible phosphoryl transfer reaction in which a tyrosine nucleophile of the enzyme attacks a phosphodiester linkage of duplex DNA, expelling the 5′-hydroxyl group of the nucleotide (Scheme 1). Thus, these unique enzymes can reversibly cleave (k_{c1}) and religate (k_r) DNA through the formation of a labile phosphotyrosine species that serves to store the energy of the original 3′−5′ phosphodiester linkage in the duplex DNA (*2*).

The simple covalent chemistry of this reaction is nature's elegant solution to altering the superhelical topology of DNA, as the nicked DNA strand is free to rotate and remove excess superhelical strain in the DNA that accumulates during DNA replication, RNA transcription, and chromosome segregation (*3*−*5*).

As with all enzymatic phosphoryl transfer reactions, the reversible cleavage chemistry of the Topo I reaction involves a finely tuned network of active site residues around the phosphoryl group, as shown in the structural model in Figure 1A for the noncovalent Michaelis complex of the human

Scheme 1

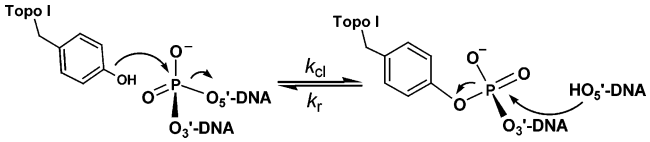

Topo with duplex DNA (PDB code 1EJ9) (*6*). In general, the largest catalytic problems that must be overcome through the use of enzyme interactions with the phosphoryl group are to accommodate the negative charge development on the nonbridging oxygens in an exploded pentacoordinate transition state and to facilitate departure of the high pK_a 5′-hydroxyl leaving group using electrostatic or general acid catalysis (*1*, *7*−*9*). Although activation of the tyrosine and 5′-OH nucleophiles through general base catalysis may also be involved, the energetic benefit from such a contribution would be expected to be smaller than leaving group activation by a general acid because model reactions of nucleophilic substitution at phosphodiester linkages show a modest dependence on nucleophile basicity ($\beta_{nuc} \sim 0.2-0.3$) and a large dependence on the basicity of the leaving group ($\beta_{lg} \sim -0.8$) (*10*, *11*). For the human enzyme, and all of the related type IB family members, the constellation of residues that appear to satisfy these catalytic roles is two arginines and a histidine that lie within hydrogen-bonding distance of the nonbridging phosphoryl oxygens and a conserved lysine and arginine positioned near the 5′-OH leaving group (Figure 1A).

Although crystallography is a powerful method to identify potentially catalytic phosphoryl−enzyme interactions, other approaches are very informative and complementary. One approach is to replace the 5′-bridging or nonbridging oxygens with sulfur and then measure the effect of sulfur substitution on a kinetic or binding parameter of the enzymatic reaction (*1*, *12*−*18*). Stereospecific substitution of a nonbridging phosphoryl oxygen with sulfur is expected to weaken an

† This work was supported by National Institutes of Health Grant GM06862-03.

* To whom correspondence should be addressed. Tel: 410-502-2758. Fax: 410-955-3023. E-mail: jstivers@jhmi.edu.

‡ The Johns Hopkins University School of Medicine.

§ Present address: The Institute for Genomic Research, 9712 Medical Center Drive, Rockville, MD 20850.

|| Polish Academy of Sciences.

[1] Abbreviations: HPLC, high-performance liquid chromatography; Tris, tris(hydroxymethyl)aminomethane; SDS, sodium dodecyl sulfate; SDS−PAGE, polyacrylamide gel electrophoresis in the presence of the denaturant SDS; Na_2EDTA, ethylenediaminetetraacetic acid disodium salt; 2-AP, 2-aminopurine; Pd, phosphodiester; Ps, phosphorothioate; R_p, phosphorothioate enantiomer with *R* configuration; S_p, phosphorothioate enantiomer with *S* configuration; TE^B, effect of bridging sulfur substitution; TE^{NB}, effect of nonbridging sulfur substitution; MALDI, matrix-assisted laser desorption−ionization mass spectrometry; hTopo, human type IB topoisomerase; vTopo, vaccinia virus type IB topoisomerase.

10.1021/bi050796k CCC: $30.25
Published on Web 08/06/2005

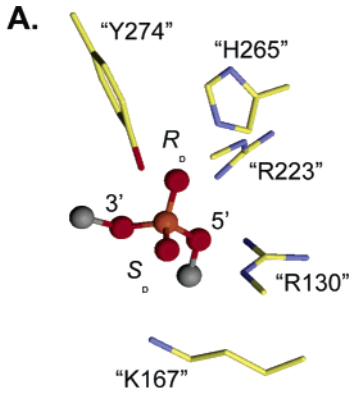

B.

Enzyme	TE^{B}	TE^{NB} Rp	TE^{NB} Sp
Wt	0.7	340	30
H265A	1.8	30	100
R130A	190		
R130K	2,600		
K167A	370		
R130K:K167A	2,000		
R223A	0.8		

FIGURE 1: Interactions of hTopo I (PDB code 1EJ9) with the scissile phosphodiester and summary of previous nonbridging and bridging thio effect measurements for vTopo. (A) A constellation of five absolutely conserved residues is observed surrounding the scissile linkage (numbering corresponds to vTopo sequence): Arg130, Lys167, Arg223, His265, and the nucleophile, Tyr274. The *proR*$_p$ and *proS*$_p$ oxygens are indicated for reference. Key distances in this precleavage complex are as follows: Arg130 NH2 → 5′-O, 2.97 Å; Arg130 NH2 → *proR*$_p$ O, 3.3 Å; Arg130 NH2 → *proS*$_p$ O, 2.56 Å; Arg223 NH1 → *proR*$_p$ O, 3.3 Å; Lys167 Nζ → 5′-O, 4 Å; His265 Nε2 → *proR*$_p$ O, 2.56 Å. (B) Summary of 5′-bridging and nonbridging thio effects (TE^{B} and TE^{NB}, respectively) (*13*, *17*, *18*). See text for further details.

enzyme interaction at that site, giving rise to an observed "thio effect" (TE), which is defined as v^{ox}/v^{S} for a velocity effect and K_a^{ox}/K_a^{S} for a binding effect. Enzymatic nonbridging thio effects (TE^{NB}) orders of magnitude *greater* than unity arise from the longer P−S bond or the lower electronegativity and altered charge distribution of sulfur as compared to oxygen, which may weaken hydrogen bonding to the sulfur substituent (*1*, *19*). In contrast, 5′-bridging thio effects (TE^{B}) can be orders of magnitude *less* than unity because of the beneficial kinetic effect of the sulfur leaving group, which has a pK_a value 5 units lower than that of the 5′-hydroxyl group (*17*, *18*).

Both bridging and nonbridging thio effects can be combined with site-directed mutagenesis of the enzyme to deduce whether a specific enzyme side chain directly or indirectly interacts with the substituted position (*13*−*15*, *17*, *18*). For instance, a mutated enzyme that lacks a side chain that interacts with a nonbridging oxygen would be expected to show a much smaller TE^{NB} than the wild-type enzyme because the mutant lacks the interaction that initially gave rise to enhanced binding of oxygen over sulfur.[2] In contrast, the activity of a mutant enzyme that lacks a general acid group to protonate the 5′-leaving oxygen would be expected to be rescued by the 5′-bridging sulfur because expulsion of the low pK_a sulfur does not require assistance from a general acid.

One type IB topoisomerase that has been especially amenable to mechanistic studies is the enzyme from vaccinia virus (vTopo) (*2*). This enzyme is distinguished by its unusually high specificity for cleavage at (C/T)CCTT↓X sites in DNA which has greatly facilitated investigation of its catalytic properties. In particular, the dual effects of bridging 5′-sulfur substitution at the cleavage site and mutagenesis of all of the key catalytic residues vTopo have been examined (Figure 1B) (*17*, *18*). This informative work revealed that when two residues of vTopo were removed by mutagenesis, Lys167 and Arg130, a large rescue by the 5′-sulfur was observed. Interestingly, the largest effect was for the R130K mutation (2600-fold), while the R130A and K167A mutations showed 10-fold smaller rescue effects (Figure 1B) (*17*, *18*). In contrast, a bridging sulfur had no effect on the DNA cleavage reactions of the wild-type enzyme or the remaining two active site deletion mutants, H265A and R223A. Taken in their entirety, these data supported a mechanism in which Lys167 and Arg130 were involved in protonating the leaving group but did not distinguish which of these groups interacted directly with the 5′-oxygen.[3] Complementary nonbridging thio effect measurements have been performed on the wild-type enzyme and the H265A mutant, confirming that His265 does not serve to protonate the leaving group but instead interacts directly with the *proR*$_p$ nonbridging oxygen in the transition state for DNA cleavage (i.e., the H265A mutant showed an 11-fold diminished R_p thio effect) (Figure 1B) (*13*). Recently, a similar study was performed using methylphosphonate substitution and mutagenesis of Arg223 to elucidate the role of this group in the transition for cleavage (*20*). Key unresolved questions are the transition-state interactions of the remaining active site groups with the nonbridging oxygens and the identity of the direct proton donor to the 5′-oxygen.

In this study, for the first time we elucidate the complete ground-state *and* transition-state interactions of vTopo with the nonbridging phosphoryl oxygens using nonbridging thio effect measurements and mutagenesis approaches. The results are used to construct an interaction map that reveals both direct and indirect energetic couplings between active site groups and the phosphoryl oxygens. The transition-state model that is suggested by the data extends our understanding of the catalytic phosphoryl interactions and is also consistent with both crystallographic distance constraints and the previous bridging thio effect measurements.

MATERIALS AND METHODS

Enzymes. Wild-type vaccinia topoisomerase was overexpressed from *Escherichia coli* strain BL21(DE3) transformed with the T7-based expression plasmid pET21-topo and purified to homogeneity using phosphocellulose chro-

[2] Nonbridging thio effects for nonenzymatic nucleophilic substitution at phosphodiester linkages fall in the range 4−11 (*1*), which suggests a lower limit for the thio effect when enzyme interactions with the nonbridging positions are completely removed by mutagenesis. Interestingly, after mutation, some of the enzymatic thio effects reported here are reduced to this range or even further (Table 2).

[3] The crystal structure of hTopo shows that NH2 of Arg488 (equivalent to Arg130 of vTopo) is 2.97 Å from the 5′ bridging oxygen, while the side chain amino group of Lys532 (equivalent to Lys167 of vTopo) is 4 Å away from the bridging oxygen (see Figure 1A; PDB code 1EJ9). Lys532 is even further away from the nonbridging oxygen in another structure of hTopo (4.64 Å; PDB code 1A36).

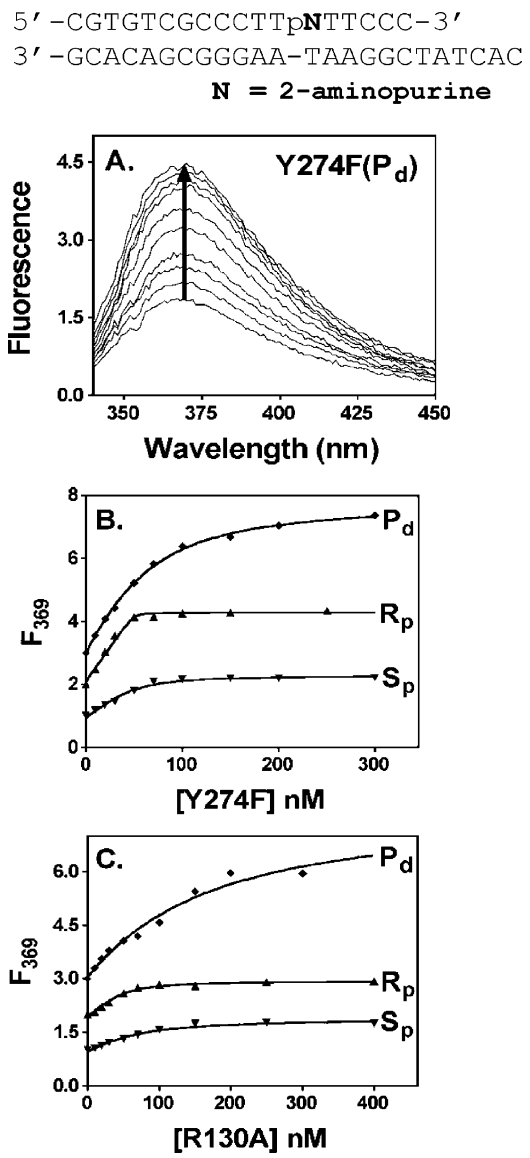

FIGURE 2: Determination of noncovalent binding affinity of Y274F topoisomerase for the normal and sulfur-substituted 18/24-mer containing a 2-aminopurine fluorescent reporter group. (A) Enzyme binding to the phosphodiester substrate (Pd) produces a 2.5-fold increase in 2-aminopurine fluorescence. (B) Binding isotherms for the Pd and the R_p and S_p sulfur-containing substrates. K_D values were 28 ± 3 nM (Pd), 1.4 ± 0.4 nM (R_p), and 9 ± 3 nM (S_p). (C) Representative titrations using the R130A mutant topoisomerase. K_D values were 80 ± 29 nM (Pd), 9 ± 4 nM (R_p), and 80 ± 20 nM (S_p). In all panels the enzyme concentration was in the range 10−300 nM.

matography as previously described (*21*). The Y274F mutant was generated using the QuickChange double-stranded mutagenesis kit obtained from Stratagene (La Jolla, CA). The mutation was confirmed by DNA sequencing of both strands of the construct, and the expressed protein was purified in a fashion identical to that for the wild-type enzyme. The mutant topoisomerases were expressed and purified as previously described (*13*). The concentration of all enzymes was determined by UV absorption measurements at 280 nm (*22*). T4 polynucleotide kinase was from New England BioLabs (Beverly, MA).

Oligonucleotide Substrates. The sequences of the phosphodiester and phosphorothioate substrates used in these studies are shown in Figure 2. The phosphodiester oligonucleotides were synthesized using standard phosphoramidite chemistry on an ABI 394B synthesizer (Applied Biosystems) at the 1.0 μmol scale. The 18-mer Ps oligonucleotides containing the fluorescent base, 2-aminopurine (2-AP), were synthesized using the commercially available 2-AP phosphoramidite reagent (Glen Research, Sterling, VA). A single phosphorothioate modification in the 2-AP-containing oligonucleotide was introduced at the CCCTTPs(2-AP) sequence using S-Tetra reagent (Glen Research, Sterling, VA), and the resulting R_p and S_p diasteromers were separated by RP-HPLC on a C18 column (Hypersil, 4.6 mm × 25 cm) as previously described (*13*). The R_p-Ps and S_p-Ps oligonucleotides used in this work were of >99% stereochemical purity (*13*). Chemical purity and structural confirmation was determined by analytical RP-HPLC analysis on a Hypersil C18 column, electrophoresis using a denaturing 20 wt % polyacrylamide gel, and MALDI-TOF. The concentrations of the single-strand oligonucleotides were determined from the pairwise extinction coefficients at 260 nm of the individual nucleotides (*23*). The strands containing the scissile bond were 5′-^{32}P end-labeled using [γ-^{32}P]ATP in the presence of T4 polynucleotide kinase, purified on Biospin-6 columns (Bio-Rad), and then hybridized to the complementary strand supplied in a 2-fold excess. For determining the site of cleavage for the Pd, R_p-Ps, and S_p-Ps 18/24-mer substrates, the 18-mer strands containing the scissile bond were 3′-^{32}P end-labeled using [α-^{32}P]ddATP in the presence of terminal deoxynucleotidyl transferase and then hybridized and purified as described above.

2-Aminopurine Fluorescence Assay for Noncovalent DNA Binding. The noncovalent binding affinity of topoisomerase for the Pd- and Ps-substituted 18/24-mer duplexes containing the fluorescent reporter group 2-aminopurine (2-AP) 3′ to the cleavage site (Figure 2) was determined by monitoring the fluorescence intensity increase at 370 nm as the enzyme binds (*24*). To prevent cleavage of the DNA, the Y274F mutant topoisomerase was used in these measurements. Measurements were made using a Spex Fluoromax-3 fluorometer (ISA Instruments) with excitation at 315 or 320 nm, excitation and emission slit widths of 4 nm, and an emission scan range of 335−450 nm. These measurements were made using a buffer consisting of 50 mM Tris (pH 7.5), 100 mM NaCl, and 1 mM DTT and a DNA concentration of 50 nM. The fluorescence data were fitted to the equation

$$F = F_0 - [(F_0 - F_f)/2[\mathrm{DNA}]_{tot}\{b - \mathrm{sqrt}(b^2 - 4[\mathrm{E}]_{tot}[\mathrm{DNA}]_{tot})\}] \quad (1)$$

where F_0 and F_f are the initial and final fluorescence values, respectively, and $b = 1/K_A + [\mathrm{E}]_{tot} + [\mathrm{DNA}]_{tot}$. The reported association constants (K_A) are the average of three replicate measurements.

Single-Turnover Cleavage Kinetics. Cleavage experiments were performed with the 18/24-mer "suicide" cleavage substrates (see Figure 2) using single-turnover conditions. In these experiments, the enzyme was always present in a 7−11-fold excess over the DNA so that the observed kinetics were pseudo first order. Cleavage experiments were performed using a 200 μL reaction volume containing 1 μM enzyme and 90−150 nM 5′-^{32}P-labeled 18/24-mer DNA in

Table 1: Mutational Effects on DNA Binding and Cleavage[a]

enzyme	K_a[b] ($\times 10^{-9}$ M^{-1})	v_i[c] (nM/h)	ME^K (K_a^{mut}/K_a^{Y274F})	ME^{cl} ($\times 10^7$) (v^{mut}/v^{wt})
		Pd		
WT (Y274F)	0.04 ± 0.004	$(7.16 \pm 0.47) \times 10^5$		
R130A			0.25 ± 0.13	2.4 ± 0.3
R130K			0.75 ± 0.20	7.1 ± 1.1
K167A			0.50 ± 0.11	111 ± 18
R223A			0.25 ± 0.08	7.0 ± 0.6
H265A			ND	0.8 ± 0.1[d]
R130A:K167A			0.8 ± 0.6	0.7 ± 0.1
R130K:K167A			0.2 ± 0.15	0.8 ± 0.1
		R_p		
WT (Y274F)	0.71 ± 0.20	1584 ± 155		
R130A			0.15 ± 0.08	126 ± 14
R130K			0.35 ± 0.21	315 ± 36
K167A			0.09 ± 0.05	252 ± 35
R223A			0.14 ± 0.08	189 ± 26
H265A			ND	13 ± 2[d]
R130A:K167A			0.15 ± 0.07	38 ± 7
R130K:K167A			0.1 ± 0.01	13 ± 13
		S_p		
WT (Y274F)	0.11 ± 0.04	$(1.01 \pm 0.06) \times 10^4$		
R130A			0.09 ± 0.04	288 ± 20
R130K			1.54 ± 1.15	417 ± 39
K167A			0.09 ± 0.05	60 ± 7
R223A			0.09 ± 0.05	20 ± 3
H265A			ND	0.6 ± 0.06[d]
R130A:K167A			0.2 ± 0.1	8 ± 0.8
R130K:K167A			0.6 ± 0.4	9 ± 1

[a] Binding and cleavage measurements were performed at 25 and 37 °C, respectively [50 mM Tris (pH 7.5), 100 mM NaCl, and 1 mM DTT]. [b] Equilibrium association constants were measured using the Y274F mutant to calculate ME^K. [c] For calculation of ME^{cl}, cleavage rate constants were measured using wild-type and mutant vTopo. [d] Previously reported (*13*).

a buffer consisting of 50 mM Tris (pH 7.5), 100 mM NaCl, and 1 mM DTT. At various time intervals 12 μL aliquots from the reaction mixture were removed and quenched in 12 μL of 2× agarose gel loading buffer containing 2% SDS. These samples were electrophoresed on a polyacrylamide gel containing 10% SDS, and the fraction of covalent complex formed at each time point was calculated and plotted against time, and the initial rates (v_i) for each reaction were calculated from the linear slopes. Cleavage experiments for the reaction of WT/P_d/24-mer at 37 °C were performed using a Kin-Tek rapid chemical quench-flow apparatus as described (*22*, *24*). These reactions were quenched at times ranging from 2.5 ms to 10 s using 10% SDS delivered from the quench syringe. For the reactions of WT enzymes with phosphorothioate substrates the reactions were initated and quenched using a hand-held pipetman, and accurate quenching times were achieved using an electronic metronome (*24*). The concentrations of DNA and the enzyme used in these experiments were 100 nM and 1 μM, respectively. The reported cleavage rates (k_{cl}) and thio effects are the average of three replicate determinations.

RESULTS

Mutational Effect Measurements. Although the substantial catalytic defects arising from the R130A(K), K167A, R223A(K), and H265A(Q) mutations have been previously reported (summarized in ref *2*), the present measurements are made using a higher NaCl concentration (100 mM), requiring new measurements. The higher salt concentrations in the buffer used here and in a previous study merely serve to weaken DNA binding to the wild-type enzyme (and the Y274F mutant), allowing measurements of DNA binding by following the increase in fluorescence of a 2-aminopurine probe (Figure 2) (*24*). Importantly, these new buffer conditions have no effect on the maximal single-turnover cleavage rate of the wild-type enzyme as compared to the standard conditions with no added NaCl (*24*, *25*). For binding affinity measurements, the Y274F mutant is used as a surrogate for the wild-type enzyme to avoid contributions from covalent chemistry (Figure 2). Previous studies have established that the specific DNA binding affinity of the Y274F mutant is very similar to that of the wild-type enzyme (*24*).

Mutational Effects on Binding to the Pd 18/24-mer. There have been no measurements to establish the roles of Arg130, Lys167, and Arg223 in specific DNA binding. We have now investigated these roles by measuring the binding affinities of the R130A, R130K, K167A, R223A, R130A:K167A, and R130K:K167A mutants to Pd and Ps containing DNA using the 2-aminopurine fluorescence assay (see panels B and C of Figure 2 for representative data). As reported in Table 1, we find that the damaging mutational effects on DNA binding (ME^K, defined as K_a^{mut}/K_a^{wt}) are modest (~2−11-fold). Thus, none of these essential residues plays a major role in stabilizing the ground-state complex prior to cleavage, suggesting that their role is to interact strongly with the transition state.

Mutational Effects on Cleavage of the Pd 18/24-mer. Measurement of the mutational effects on cleavage at 37 °C required a rapid kinetic investigation of the wild-type reaction (Figure 3A). The maximal cleavage rate for the phosphodiester substrate was 2.0 ± 0.1 s^{-1}, which is 5−7 times faster than previous reports (*17*, *20*). Approximately 3-fold of this

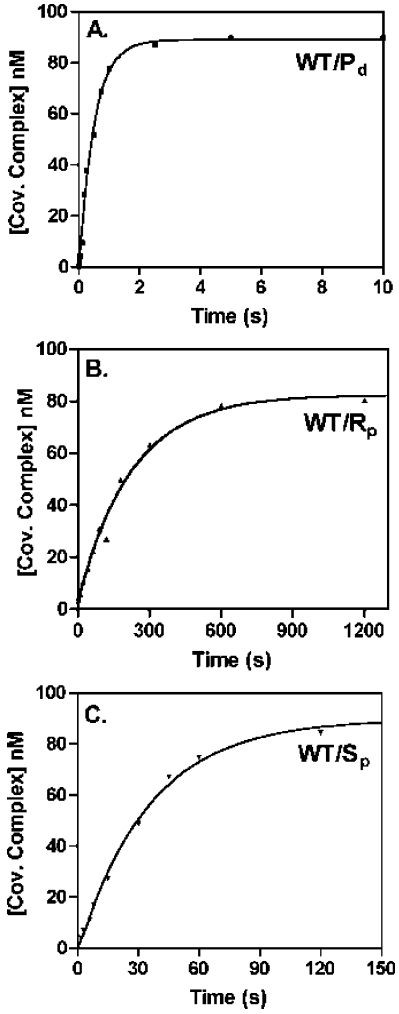

FIGURE 3: Thio effects on DNA cleavage for wild-type vTopo at 37 °C. (A) Reaction of 1 μM wt vTopo with 100 nM Pd 18/24-mer using a rapid chemical quench-flow apparatus ($k_{cl} = 2 \pm 0.1$ s^{-1}). (B) Reaction of 100 nM R_p 18/24-mer with 1 μM vTopo ($k_{cl} = 0.004 \pm 0.0004$ s^{-1}). (C) Reaction of 100 nM S_p 18/24-mer with 1 μM vTopo ($k_{cl} = 0.03 \pm 0.002$ s^{-1}). Curves are nonlinear regression fits to the equation $[P]_t = [P]_\infty(1 - e^{-kt})$, where $[P]_t$ is the concentration of covalent complex at time t and $[P]_\infty$ is the concentration at infinite time.

discrepancy may be attributed to the enhanced cleavage rate for substrates containing a 2-aminopurine nucleotide in the position immediately 3′ to the cleavage site (previous studies had an A in this position) (*24*). The remaining ~2-fold difference is likely attributed to the manual quench methods previously employed, which precluded measurement of much of the reaction time course. In contrast with the modest effects on DNA binding, rate measurements of DNA cleavage by each of the mutants revealed profound mutational effects in the range 10^{-7} to 10^{-5} for the Pd 18/24-mer [the mutational effect (ME^{cl}) is defined as v^{mut}/v^{wt}; see Table 1]. These findings are consistent with previous mutagenesis studies of vTopo (summarized in ref *1*).

Thio Effects on 18/24-mer Binding. The effects of stereospecific sulfur substitution on ground-state DNA binding by the Y274F, R130A, R130K, K167A, R223A single mutants and the R130A:K167A and R130K:K167A double mutants were also measured using the 2-aminopurine fluorescence assay (Figure 2B,C and Table 2). Surprisingly, the R_p sulfur substitution resulted in 3−11-fold *tighter* binding ($K_a^{ox}/K_a^S < 1$) for all of the enzymes tested. In contrast, S_p sulfur substitution had a much smaller effect on binding for all of the enzymes except for R130K, which showed 7-fold tighter DNA binding for this enantiomer ($K_a^{ox}/K_a^S = 0.18$). These results are surprising in light of the expectation that nonbridging sulfur substitution should weaken or have no effect on DNA binding affinity in systems where chelation of a divalent cation is not involved (*26*). However, there is precedence for sulfur substitution leading to enhanced ground-state DNA binding for several diverse protein−DNA interactions such as *Eco*RI restriction enzyme and uracil DNA glycosylase (*14*, *27*). To our knowledge there are no examples of enhanced transition-state binding upon substitution of a nonbridging oxygen with sulfur, likely due to the more rigid geometric and electrostatic requirements in the transition state. These broad findings suggest that the localized negative charge on the sulfur atom, as opposed to the delocalized negative charge on the nonbridging oxygens, may in certain cases give rise to enhanced ground-state electrostatic interactions with enzymes that interact with the anionic backbone of DNA. Consistent with this interpretation, we have previously observed that K_a^{ox}/K_a^S for Y274F approaches unity when the binding measurements are performed at high ionic strength (200 mM NaCl) where electrostatic interactions are screened (*13*). A general conclusion that emerges from the mutagenesis and thio effect measurements on DNA binding is that nonspecific electrostatic interactions are substantial around the R_p sulfur of the

Table 2: Thio Effects on DNA Binding and Cleavage[a]

DNA	TE^K (K_a^{ox}/K_a^S)	TE^{cl} (v^{ox}/v^S)	TE_{cl}^{rel} ($TE_{cl}^{wt}/TE_{cl}^{mut}$)
		WT	
R_p	0.06 ± 0.02	450 ± 55	
S_p	0.36 ± 0.14	70 ± 6	
		R130A	
R_p	0.09 ± 0.06	9 ± 1	50 (31)[b]
S_p	1 ± 0.6	0.6 ± 0.1	117 (15)
		R130K	
R_p	0.12 ± 0.07	11 ± 2	42
S_p	0.18 ± 0.12	1 ± 0.2	70
		K167A	
R_p	0.33 ± 0.18	199 ± 34	2 (4)
S_p	2 ± 1	132 ± 22	0.5 (0.4)
		R223A	
R_p	0.1 ± 0.06	16 ± 1	28 (21)
S_p	1 ± 0.5	25 ± 3	3 (2)
		H265A[d]	
R_p		(30 ± 4)	(11)
S_p		(100 ± 12)	(0.3)
		R130A:K167A	
R_p	0.3 ± 0.2	8 ± 2	56
S_p	1.5 ± 1.3	6 ± 1	12
		R130K:K167A	
R_p	≤3.3	30 ± 24	15
S_p	≤0.2	7 ± 1	10

[a] Binding and cleavage measurements were performed at 25 and 37 °C, respectively, using a buffer consisting of 50 mM Tris (pH 7.5), 100 mM NaCl, and 1 mM DTT. [b] Parenthetical values are for cleavage measurements made at 25 °C. [c] The temperature dependence of the thio effect could reflect a strong enthalpic interaction of Arg130 with the S_p oxygen that is absent with the S_p sulfur. The TE_{cl}^{rel} is large at both temperatures; thus the conclusions are not dependent on this temperature dependency. [d] Previously reported (*13*).

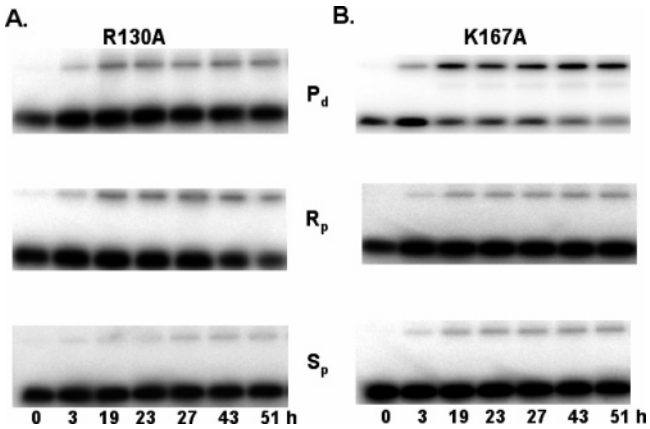

FIGURE 4: Gel analysis of the initial rate time course for covalent complex formation for the R130A and K167A mutant enzymes using the Pd and the R_p and S_p sulfur-containing substrates. The lower band is the DNA substrate, and the upper band that appears with time is the covalent enzyme−DNA complex. The reactants and products are separated by electrophoresis using a 10% polyacrylamide gel containing SDS.

scissile phosphodiester linkage and that the entire cluster of positively charged groups contributes to these ground-state effects (Arg130, Lys167, and Arg223). Accordingly, the R_p thio effects are largest for Y274F, which possesses all of these groups, and are diminished to varying degrees for nearly all of the other mutants.

Thio Effects on 18/24-mer Cleavage. The site-specific cleavage kinetics of the vaccinia enzyme are usually studied using single-turnover conditions with limiting DNA and excess enzyme, and the progress is monitored by resolution of the free 5′-^{32}P DNA from the phosphotyrosine covalent adduct using SDS−PAGE. The complete time course for conversion of free labeled substrate to the covalently bound form is followed, and the data are fitted to a single exponential rate equation to obtain the pseudo-first-order rate constant for cleavage (k_{cl}). Such measurements for the wild-type enzyme with the Pd, R_p, and S_p substrates are shown in panels A, B, and C of Figure 3, respectively (T = 37 °C). The thio effects calculated from these data are 450 and 70 for the R_p and S_p substrates, which are slightly larger than the previous R_p and S_p thio effect measurements of 340 and 30, measured at 25 °C (see Figure 1) (*13*).

With severely handicapped mutants, such as those studied here, it is impossible to follow the entire time course of the reaction, and accordingly, initial rate measurements were required. The SDS−PAGE analyses of the initial rate time courses for the phosphodiester and phosphorothioate DNA cleavage reactions catalyzed by the R130A and K167A mutants are shown in panels A and B of Figure 4, respectively. From simple visual inspection of these data, it is readily apparent that the K167A mutant has a large and nearly equal TE^{NB} for both the R_p and S_p substrates and that the TE^{NB} for R130A is much smaller and stereospecific (the ratio of the TE^{NB} for R130A is R_p/S_p = 9; see Table 2). The initial rate data for these and the other reactions were fitted by linear regression to obtain v^{ox} and v^{S} (Figure 5 and Table 2). One exception was the more rapid reaction of K167A, which allowed fitting to a first-order rate equation (Figure 5B).

Because these mutations and thio substitutions result in severe rate defects, it was essential to perform a control

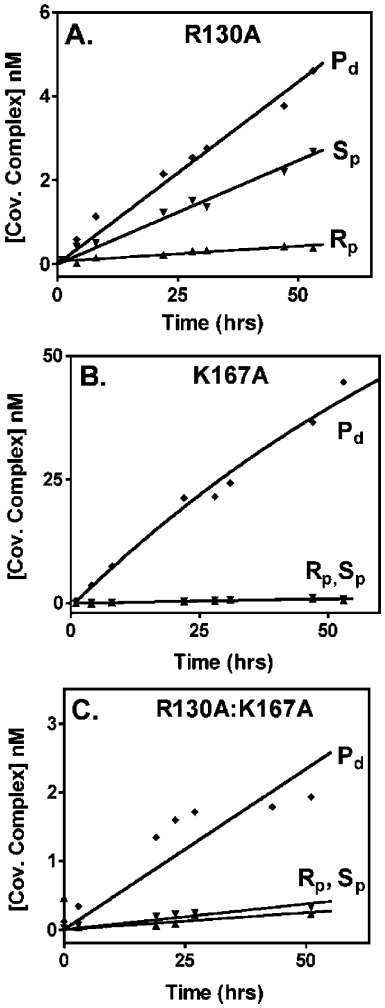

FIGURE 5: Initial rates of covalent complex formation for the R130A, K167A, and R130A:K167A topoisomerase mutants. (A) Reaction of the R130A enzyme with Pd and S_p and R_p substrates. (B) Reaction of the K167A enzyme with Pd and S_p and R_p substrates. (C) Reaction of the R130A:K167A enzyme with Pd and S_p and R_p substrates. These representative data were obtained at reaction temperatures of 25 °C (A and B) and 37 °C (C).

experiment to establish that all of the mutant enzymes cleaved each DNA substrate at the normal site of cleavage (i.e., CCCTT↓X). This was ascertained by 3′-end labeling the scissile strand with 3′-[α-^{32}P]ddATP and then resolving the expected 7-mer product of the cleavage reaction on a denaturing 20% polyacrylamide gel containing 7 M urea. In all cases the expected 7-mer was the only cleavage product observed (not shown). In addition, to confirm that the nonbridging thio effects on cleavage were not salt concentration dependent, we repeated the velocity measurements with the R130A mutant in the absence of NaCl and obtained similar results as reported in Table 2 for the 100 mM salt conditions [TE (R_p) = 9 ± 1, TE (S_p) = 1.9 ± 0.3].

The most important parameters reported in Table 2 are the relative thio effects as compared to the wild-type enzyme (TE^{rel} = TE^{wt}/TE^{mut}). Conservative rules of thumb for interpretation of the kinetic TE^{rel} values are that (i) a value close to unity indicates that a given side chain does not form a substantial interaction with a nonbridging position, (ii) a $TE^{rel} \gg 1$ indicates a potential direct interaction between the wild-type side chain and a nonbridging position, and (iii) a $TE^{rel} < 1$ indicates that removal of a side chain gives rise

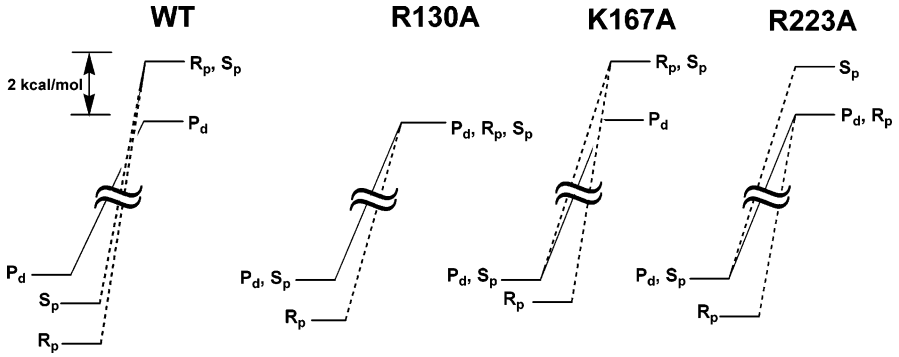

FIGURE 6: Energetic effects of sulfur substitution in the ground state and transition state for DNA cleavage. Thio effects on binding and the activation barrier for cleavage were converted into difference free energy changes using the simple relationships $\Delta\Delta G_{bind} = -RT \ln TE^{K}$ and $\Delta\Delta G_{cl} = -RT \ln TE^{cl}$. The change in the transition-state energy as a result of thio substitution for each mutant ($\Delta\Delta G^{\ddagger}$) was calculated using the equation $\Delta\Delta G^{\ddagger} = \Delta\Delta G_{cl} - \Delta\Delta G_{bind}$. For scaling, the bar on the left shows a free energy change corresponding to 2 kcal/mol. The differences between the ground-state and transition-state energy levels for each substrate correspond to the bar scale, but the overall activation barrier heights are truncated in the diagram for simplicity (≈).

to enhanced binding of sulfur as compared to oxygen, which could be a direct or indirect effect (see Discussion). As discussed above, the relative thio effects on DNA binding appear to be driven by long-range electrostatic interactions with the less delocalized sulfur anion. All thio effect interpretations are best evaluated by keeping in mind the structural constraints of the ground state obtained from crystallographic measurements (Figure 1A), the effects of mutagenesis alone, and the structural constraints imposed by a pentacoordinate transition state. Moreover, measuring a complete family of thio and mutagenesis effects provides more confidence than the measurement of a single effect alone. We interpret the TE^{rel} values for each mutant in the following discussion.

DISCUSSION

Dissecting the Energetics of Sulfur Substitution

Thio Effects on Binding and Cleavage for Wild-Type vTopo. Thio effects on binding and cleavage may be converted into difference free energy changes using the simple relationships $\Delta\Delta G_{bind} = -RT \ln TE^{K}$ and $\Delta\Delta G_{cl} = -RT \ln TE^{cl}$. Thus, with independent measurements of the effects of sulfur substitution on binding and the activation barrier, it is possible to dissect the overall effect on the cleavage activation barrier into ground-state and transition-state contributions as depicted in the free energy profiles in Figure 6. For wild-type vTopo, R_p sulfur substitution leads to an overall 3.6 kcal/mol increase in the cleavage activation barrier, which is comprised of a 1.7 kcal/mol ground-state stabilization and a 1.9 kcal/mol destabilization of the transition state for cleavage (Figure 6). In contrast, the S_p sulfur substituent has little effect on ground-state binding but produces an identical 1.9 kcal/mol destabilization in the transition state. These findings suggest that the R_p sulfur anion (but not the S_p) interacts favorably in the ground state with the cluster of positively charged residues defining the active site. When the transition-state conformation is reached, an additional interaction with the S_p position becomes important. These results define a pathway for forming the transition state that involves an initial loose organization of enzyme groups around the phosphodiester linkage in the ground state involving, at least in part, long-range electrostatic attraction with the R_p substituent. More extensive interactions with the phosphoryl group then ensue as the transition-state conformation is attained.

R130A(K). Removal of Arg130 only slightly lessens the R_p thio effect in the ground state as compared to the wild-type enzyme but essentially abolishes the interaction giving rise to the R_p and S_p thio effect in the transition state (Figure 6). These thio effect results are completely consistent with the observed interactions of Arg130 in the precleavage complex (Figure 1), where its side chain NH2 forms a bifurcated hydrogen bond with both of the nonbridging oxygens.

An additional interesting finding with R130A is that the R_p thio effect on the cleavage activation barrier arises entirely from ground-state stabilization (Figure 6), whereas the wild-type enzyme shows both ground-state stabilization and transition-state destabilization effects (Figure 6). It would appear that removal of Arg130 disrupts all of enzyme interactions with the R_p position in the transition state (including the interactions of His265 and Arg223). Such a scenario would explain the especially large damaging effect of the R130A mutation. Since the R130K mutation has the same damaging effect on the cleavage rate as R130A and, in addition, produces similar nonbridging thio effects (Tables 1 and 2), then the Lys130 amino group must not interact with either of the nonbridging oxygens. This is a reasonable result as the shorter lysine side chain is unable to extend out far enough to make these interactions.

K167A. The structure of human Topo shown in Figure 1 (PDB code 1EJ9) indicates that the side chain amino group of Lys167 is located 3.2 Å from the *pro*S_p oxygen. Removal of Lys167 elicits 7- and 5-fold weaker binding to the S_p and R_p sulfurs in the ground state as compared to the wild-type enzyme (Table 2, Figure 6), suggesting that Lys167 directly or indirectly affects electrostatic interactions with these positions. In the transition state, removal of Lys167 causes a 5-fold increase in the thio effect for the S_p substrate as compared to wild-type Topo, corresponding to a 1.5 kcal/mol increase in the transition-state energy (Figure 6). This result indicates that in the *absence* of Lys167 a stronger interaction with the *pro*S_p oxygen in the transition state exists. Since both structural and thio effect measurements indicate that Arg130 is the only other residue that directly contacts the *pro*S_p oxygen, then a likely scenario is that the Arg130−*pro*S_p oxygen interaction is stronger when electrostatic

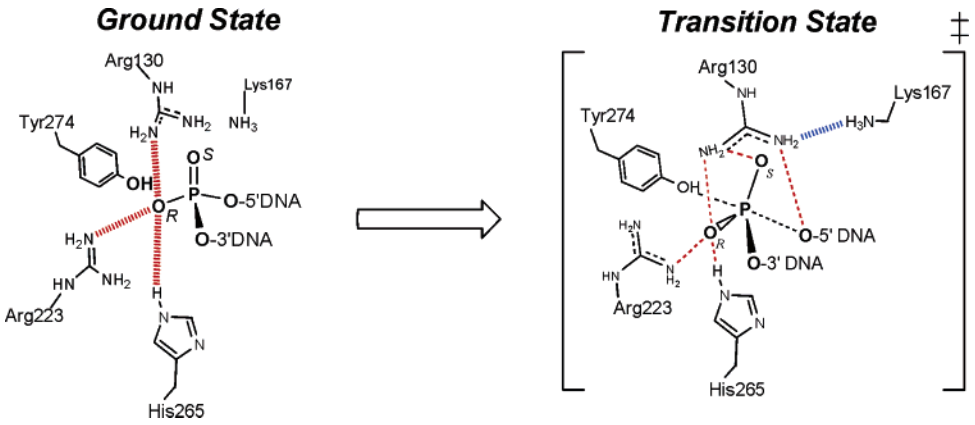

FIGURE 7: Ground-state and transition-state interactions of vTopo with the reactive phosphoryl group as deduced from thio effect and structural studies (see text).

repulsion by the nearby Lys167 is removed. This finding provides strong evidence for thermodynamic linkage between Arg130 and Lys167, as suggested previously (*18*).

R223A. Removal of Arg223 causes a stereoselective 28-fold decrease in the R_p thio effect on cleavage but has little effect on the S_p thio effect (Table 2). These effects reflect weaker ground-state and transition-state interactions with the R_p sulfur in the absence of Arg223 and the absence of an interaction of Arg223 with the S_p position (Figure 6). A direct interaction of Arg223 with the R_p position is in complete accord with the crystal structure shown in Figure 1 and recent measurements using stereospecific methylphosphonate substitutions at the cleavage site (*20*).

Double Mutations R130A:K167A and R130K:K167A. Both of these double mutations give rise to very similar rate defects and changes in thio effects as compared to wild-type Topo (Table 1). The R_p thio effect is in the range 8−30 for these double mutants, which is similar to the R130A or R130K mutations alone. This reaffirms the conclusion that Lys167 has no direct or indirect effect on enzyme interactions with the R_p substituent. For both double mutants, the S_p thio effect is smaller by 22-fold as compared to the K167A single mutant, which is the expected result if the presence of Lys167 indirectly weakens the interaction of Arg130 with the S_p substituent as suggested above.

Structural Interpretations

Deducing Ground-State and Transition-State Interaction Maps. The thio effects describe a web of direct and indirect interactions that allow the construction of structures of the ground state and the pentacoordinate transition state for cleavage (Figure 7). The nonbridging thio effects on DNA binding, which indicate enhanced binding to the R_p sulfur as compared to oxygen, strongly suggest that electrostatic interactions with the R_p position are prevalent in the ground state (hashed lines, Figure 7). As would be expected, removal of any of the cluster of cationic groups in the active site diminishes the R_p interaction (lowers the thio effect), indicating that long-range electrostatics are used to nucleate the formation of the precleavage complex. These conclusions are supported by the strong salt dependence of the thio effect on binding, which essentially disappears at 200 mM NaCl concentration (*13*). Previous studies have established the presence of three conformational states of the enzyme−DNA complex prior to cleavage that are interconverted in a rapid equilibrium process (*24*, *25*). Thus the thio effects are a population-weighted average for all of these bound states. These conformational states may explain the differences in positions of active site groups observed in two crystal structures of the noncovalent complex of the human enzyme with DNA (PDB codes 1EJ9 and 1A36) (*6*, *28*). The structure depicted in Figure 1 (PDB code 1EJ9) is likely to be farther along the reaction coordinate for phosphoryl transfer than 1A36 because the active site groups are more closely positioned around the scissile phosphorus. Therefore, we use this structure for comparison with the thio effect measurements (see footnote 3 for a description of some of the structural differences in these complexes).

Many of the ground-state interactions are preserved in the transition state, but Arg130 appears to take on a more extensive scaffolding role in the transition state. The apparent monodentate interaction of Arg130 with the R_p position in the ground state is replaced with a bifurcated hydrogen bond between both the R_p and S_p oxygens in the transition state (Figure 7). This single bifurcated hydrogen bond is significantly different than the previous proposal of a bidentate hydrogen bond involving both side chain NH2 groups of Arg130. This bidentate arrangement was assumed on the basis that the catalytic role of Arg130 could not be mimicked by substituting lysine at this position (*29*−*31*). However, we no longer favor this arrangement for two reasons. First, a bidentate interaction would require a significant conformational change in the side chain of Arg130 as the transition state is approached, as may be inferred from the crystal structure in Figure 1. Second, it is difficult to rationalize the large rate rescue of a 5′-bridging sulfur for the R130A mutant (190-fold) and the even larger rescue of 2600-fold for the R130K mutant if both NH2 groups are interacting with the nonbridging oxygens (Figure 1) (*17*, *18*). These significant bridging sulfur rescues strongly suggest that Arg130 is involved directly or indirectly in leaving group expulsion. Such a role for Arg130 would require that its second guanidinium group be available for this interaction as indicated in Figure 7 (see discussion below). The remaining transition-state interactions involve hydrogen bonding of Arg223 and His265 to the R_p oxygen and a proposed through-space electrostatic repulsion between Lys167 with Arg130. As described above, this strained interaction is suggested by the increased S_p thio effect when Lys167 is removed, indicating that Arg130 interacts more strongly with the S_p

oxygen in the absence of Lys167. These interactions, which are inferred entirely from the thio effect measurements, are consistent with the positions of these groups in the ground-state crystal structure of the human enzyme shown in Figure 1.

Is Arg130 or Lys167 the General Acid? Previous 5′-bridging thio effect measurements have led to the conclusion that Lys167 and Arg130 are important for 5′-OH leaving group explusion but were ambiguous with respect to which group directly interacts with the 5′ position (*17*, *18*). A key experimental observation that needs to be accounted for to understand the role of these two groups is the large 2600-fold 5′-sulfur rescue of the R130K mutant, which is 14 times greater that the R130A mutationand 7 times greater that the K167A mutation. This large rescue is curious because removal of the true general-acid group would be expected to result in the largest 5′-sulfur rescue, *but neither the R130A or K167A mutations result in as large a rescue as R130K*.

Even after completion of these nonbridging thio effect and mutagenesis measurements it is difficult to confidently conclude whether Arg130 or K167 is the direct proton donor to the 5′-leaving oxygen. Nevertheless, these data allow the construction of a plausible model that accounts for the large bridging thio effect for R130K. In this model (Figure 8), we assume that Arg130 is the direct donor and that Lys167 plays a secondary role in positioning Arg130 or in modulating its pK_a. We make this assumption solely on the basis that Arg130 is closer to the 5′-leaving group oxygen in several crystal structures (*6*, *28*), while Lys167 is always farther away. If this assumption is not correct, then the model still holds, but the roles for Arg130 and K167 in Figure 8 are reversed.[3]

For the wild-type enzyme (Figure 8A), Arg130 interacts with both the nonbridging and bridging oxygens: its interaction with the nascent negative charge on the 5′-leaving oxygen is presumed to be enhanced by the presence of Lys167, which may serve to lower the pK_a of Arg130 so that it more closely matches that of the 5′-hydroxyl group (*32*, *33*). For wild-type Topo, efficient leaving group stabilization by Arg130 leads to a nonexistent 5′-sulfur rescue (Figure 8A). The suggested interaction of the two nitrogens of Arg130 with the nonbridging and bridging oxygens depicted in Figures 7 and 8 would only require a modest rotation around a side chain torsion angle as judged from the crystal structure in Figure 1, bringing its NH1 within 2.9 Å of the 5′-oxygen. Such a conformational change in Arg130 could accompany reorganization of the substrate from the ground state to the pentacoordinate transition state without a large reorganizational energy. For the R130A mutation (Figure 8B), the interaction between Arg130 and Lys167 is abrogated, allowing Lys167 to move within hydrogen-bonding distance of the 5′ leaving group, thereby acting as a less efficient surrogate general-acid catalyst. Thus, the 5′-sulfur rescue is much greater than the wild-type enzyme but 14-fold smaller than the maximal effect seen for the R130K mutant. In Figure 8C is depicted the case of the K167A mutant. In the absence of Lys167, Arg130 forms a weaker interaction with the developing negative charge on the leaving oxygen because its pK_a is no longer optimally matched to the leaving group resulting in a substantial 5′-sulfur rescue (370-fold), but significantly less than the maximal value observed for R130K. For the R130K mutation

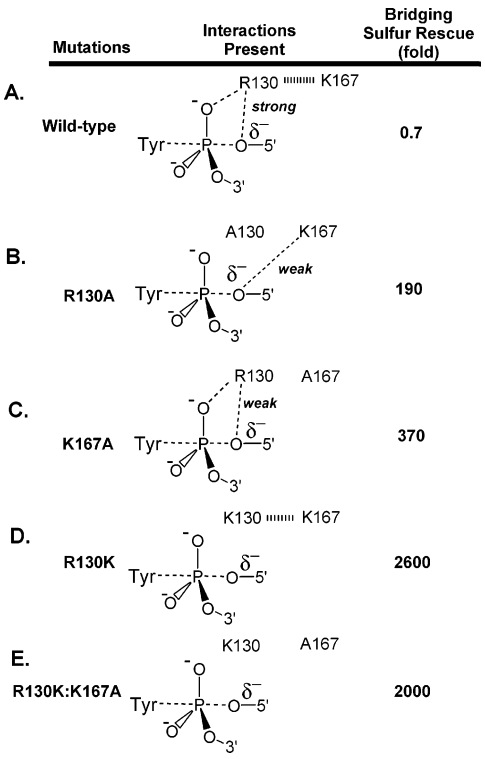

FIGURE 8: Postulated interactions between Arg130, Lys167, and the 5′-leaving oxygen based on structural studies and thio effect measurements. For clarity, Arg130 NH2 is shown to interact with only one nonbridiging oxygen in the depiction (see Figure 7 for complete interactions). The interactions indicated with each mutant topoisomerase are consistent with the observed 5′-bridging sulfur rescue effects. Weak electrophilic interactions with the 5′-oxygen as compared to the wild-type enzyme are noted for R130A and K167A. The hash mark connecting Arg130 (or Lys130) and Lys167 indicates a repulsive interaction between these groups (e.g., strain). In the case of R130K, the interaction of Lys130 with Lys167 prevents the weak contact between Lys167 and the 5′-oxygen that is allowed with the Ala130 mutation. In this depiction, Arg130 is assumed to be the direct proton donor to the 5′-leaving group oxygen, and Lys167 plays a secondary role. Consistent with this depiction, Arg130 is closer than Lys167 to this oxygen in several crystal structures (see, for instance, PDB codes 1A36 and 1EJ9). However, if this assumption is not correct, the model still holds, but the roles for Arg130 and Lys167 are reversed.

(Figure 8D), the Lys130 side chain is too short to reach the 5′-bridging oxygen or the nonbridging oxygens, but it is still able to interact with the Lys167 side chain, preventing its adventitious interaction with the 5′-oxygen as observed with the R130A mutation. Accordingly, the 5′ rescue is largest (2600-fold) for R130K and similar for the R130K:K167A double mutation (2000-fold). Although these interpretations are not without alternatives, they are most consistent with all of the thio effect and structural data. Interestingly, a role for guanidinium groups as general-acid catalysts in phosphoryl transfer has been recently established in a model system (*34*).

Conclusion. The enzyme interactions with the reactive phosphoryl group of Topo IB in the ground state and transition state have been elucidated. A key finding is the intricate interaction of Arg130 with both of the nonbridging oxygens as well as the bridging oxygen leaving group. Thus, the large damaging effect of deleting Arg130 arises from removal of multiple catalytic interactions involved in stabilization of developing negative charge on the nonbridging

oxygens and the leaving group. The pivotal role of Arg130 in leaving group stabilization is facilitated by Lys167, which may serve to lower its pK_a in the transition state.

ACKNOWLEDGMENT

We thank Dr. Stewart Shuman for providing the expression plasmids for some of the mutant enzymes used in this work.

REFERENCES

1. Herschlag, D., Piccirilli, J. A., and Cech, T. R. (1991) Ribozyme-catalyzed and nonenzymatic reactions of phosphate diesters: Rate effects upon substitutions of sulfur for a nonbridging phosphoryl oxygen atom, *Biochemistry 30*, 4844−4854.
2. Shuman, S. (1998) Vaccinia virus DNA topoisomerase: A model eukaryotic type IB enzyme, *Biochim. Biophys. Acta 1400*, 321−337.
3. Stivers, J. T., Harris, T. K., and Mildvan, A. S. (1997) Vaccinia DNA topoisomerase I: Evidence supporting a free rotation mechanism for DNA supercoil relaxation, *Biochemistry 36*, 5212−5222.
4. Champoux, J. J. (2001) DNA topoisomerases: Structure, function, and mechanism, *Annu. Rev. Biochem. 70*, 369−413.
5. Koster, D. A., Croquette, V., Dekker, C., Shuman, S., and Dekker, N. H. (2005) Friction and torque govern the relaxation of DNA supercoils by eukaryotic topoisomerase IB, *Nature 434*, 671−674.
6. Redinbo, M. R., Champoux, J. J., and Hol, W. G. (2000) Novel insights into catalytic mechanism from a crystal structure of human topoisomerase I in complex with DNA, *Biochemistry 39*, 6832−6840.
7. Admiraal, S. J., Meyer, P., Schneider, B., Deville-Bonne, D., Janin, J., and Herschlag, D. (2001) Chemical rescue of phosphoryl transfer in a cavity mutant: A cautionary tale for site-directed mutagenesis, *Biochemistry 40*, 403−413.
8. Admiraal, S. J., and Herschlag, D. (1995) Mapping the transition state for ATP hydrolysis: Implications for enzymatic catalysis, *Chem. Biol. 2*, 729−739.
9. Morrison, J. F., and Heyde, E. (1972) Enzymic phosphoryl group transfer, *Annu. Rev. Biochem. 41*, 29−54.
10. Kirby, A. J., and Younas, M. (1970) Reactivity of phosphate Esters−Reactions of diesters with nucleophiles, *J. Chem. Soc. B*, 1165.
11. Kirby, A. J., and Younas, M. (1970) Reactivity of phosphate esters − diester hydrolysis, *J. Chem. Soc. B*, 510.
12. Yoshida, A., Shan, S., Herschlag, D., and Piccirilli, J. A. (2000) The role of the cleavage site 2′-hydroxyl in the tetrahymena group I ribozyme reaction, *Chem. Biol. 7*, 85−96.
13. Stivers, J. T., Jagadeesh, G. J., Nawrot, B., Stec, W. J., and Shuman, S. (2000) Stereochemical outcome and kinetic effects of R_p- and S_p-phosphorothioate substitutions at the cleavage site of vaccinia type I DNA topoisomerase, *Biochemistry 39*, 5561−5572.
14. Werner, R. M., Jiang, Y. L., Gordley, R. G., Jagadeesh, G. J., Ladner, J. E., Xiao, G., Tordova, M., Gilliland, G. L., and Stivers, J. T. (2000) Stressing-out DNA? The contribution of serine-phosphodiester interactions in catalysis by uracil DNA glycosylase, *Biochemistry 39*, 12585−12594.
15. Hondal, R. J., Bruzik, K. S., Zhao, Z., and Tsai, M. D. (1997) Mechanism of phosphatidylinositol-phospholipase c. 2. Reversal of a thio effect by site-directed mutagenesis, *J. Am. Chem. Soc. 119*, 5477−5478.
16. Kravchuk, A. V., Zhao, L., Kubiak, R. J., Bruzik, K. S., and Tsai, M. D. (2001) Mechanism of phosphatidylinositol-specific phospholipase c: Origin of unusually high nonbridging thio effects, *Biochemistry 40*, 5433−5439.
17. Krogh, B. O., and Shuman, S. (2000) Catalytic mechanism of DNA topoisomerase IB, *Mol. Cell 5*, 1035−1041.
18. Krogh, B. O., and Shuman, S. (2002) Proton relay mechanism of general acid catalysis by DNA topoisomerase IB, *J. Biol. Chem. 277*, 5711−5714.
19. Frey, P. A., and Sammons, R. D. (1985) Bond order and charge localization in nucleoside phosphorothioates, *Science 228*, 541−545.
20. Tian, L., Claeboe, C. D., Hecht, S. M., and Shuman, S. (2005) Mechanistic plasticity of DNA topoisomerase IB: Phosphate electrostatics dictate the need for a catalytic arginine, *Structure (Cambridge) 13*, 513−520.
21. Morham, S. G., and Shuman, S. (1992) Covalent and noncovalent DNA binding by mutants of vaccinia DNA topoisomerase I, *J. Biol. Chem. 267*, 15984−15992.
22. Stivers, J. T., Shuman, S., and Mildvan, A. S. (1994) Vaccinia DNA topoisomerase I: Single-turnover and steady-state kinetic analysis of the DNA strand cleavage and ligation reactions, *Biochemistry 33*, 327−339.
23. Fasman, G. D. (1975) *Handbook of biochemistry and molecular biology: Nucleic acids*, 3rd ed., Vol. 1, CRC Press, Boca Raton, FL.
24. Kwon, K., and Stivers, J. T. (2002) Fluorescence spectroscopy studies of vaccinia type IB DNA topoisomerase. Closing of the enzyme clamp is faster than DNA cleavage, *J. Biol. Chem. 277*, 345−352.
25. Kwon, K., Jiang, Y. L., Song, F., and Stivers, J. T. (2002) ^{19}FNMR studies of vaccinia type IB topoisomerase. Conformational dynamics of the bound DNA substrate, *J. Biol. Chem. 277*, 353−358.
26. Shan, S., Kravchuk, A. V., Piccirilli, J. A., and Herschlag, D. (2001) Defining the catalytic metal ion interactions in the tetrahymena ribozyme reaction, *Biochemistry 40*, 5161−5171.
27. Lesser, D. R., Grajkowski, A., Kurpiewski, M. R., Koziolkiewicz, M., Stec, W. J., and Jen-Jacobson, L. (1992) Stereoselective interaction with chiral phosphorothioates at the central DNA kink of the EcoRI endonuclease-gaattc complex, *J. Biol. Chem. 267*, 24810−24818.
28. Stewart, L., Redinbo, M. R., Qiu, X., Hol, W. G., and Champoux, J. J. (1998) A model for the mechanism of human topoisomerase I, *Science 279*, 1534−1541.
29. Stivers, J. T., Shuman, S., and Mildvan, A. S. (1994) Vaccinia DNA topoisomerase I: Kinetic evidence for general acid−base catalysis and a conformational step, *Biochemistry 33*, 15449−15458.
30. Wittschieben, J., and Shuman, S. (1994) Mutational analysis of vaccinia DNA topoisomerase defines amino acid residues essential for covalent catalysis, *J. Biol. Chem. 269*, 29978−29983.
31. Wittschieben, J., and Shuman, S. (1997) Mechanism of DNA transesterification by vaccinia topoisomerase: Catalytic contributions of essential residues Arg-130, Gly-132, Tyr-136 and Lys-167, *Nucleic Acids Res. 25*, 3001−3008.
32. Shan, S. O., and Herschlag, D. (1996) The change in hydrogen bond strength accompanying charge rearrangement: Implications for enzymatic catalysis, *Proc. Natl. Acad. Sci. U.S.A. 93*, 14474−14479.
33. Shan, S. O., Loh, S., and Herschlag, D. (1996) The energetics of hydrogen bonds in model systems: Implications for enzymatic catalysis, *Science 272*, 97−101.
34. Piatek, A. M., Gray, M., and Anslyn, E. V. (2004) Guanidinium groups act as general-acid catalysts in phosphoryl transfer reactions: A two-proton inventory on a model system, *J. Am. Chem. Soc. 126*, 9878−9879.

BI050796K